

Predicted errors of tropospheric emission spectrometer nadir retrievals from spectral window selection

John Worden,¹ Susan S. Kulawik,¹ Mark W. Shephard,² Shepard A. Clough,²
Helen Worden,¹ Kevin Bowman,¹ and Aaron Goldman³

Received 8 January 2004; revised 1 March 2004; accepted 11 March 2004; published 15 May 2004.

[1] Error covariances and vertical resolutions are reported for Tropospheric Emission Spectrometer (TES) nadir-view retrievals of surface temperature, atmospheric temperature, H₂O, O₃, CO, and CH₄. These error covariances are computed as a result of selecting spectral windows that maximize the information content of simulated, TES nadir-view atmospheric retrievals of four regions representative of northern midlatitude, southern midlatitude, tropical, and polar climates. The information content of a retrieval is a function of an a priori and an a posteriori covariance matrix where the a posteriori covariance depends on an estimated smoothing error, measurement error, and systematic errors from interfering species, surface emissivity, atmospheric and surface temperature, and line parameter uncertainties. For conditions representative of northern midlatitudes, we can expect about 3 degrees of freedom (DOF) for retrievals of H₂O, 5 DOF for O₃ with about 2.4 DOF in the troposphere, and 0.8 DOF for CO. These measures for the vertical resolution and the predicted errors can be used to assess which atmospheric science questions can be addressed with TES atmospheric retrievals. Proper characterization of TES retrievals is also critical for applications such as atmospheric data assimilation and inverse modeling. *INDEX TERMS:* 0365 Atmospheric Composition and Structure: Troposphere—composition and chemistry; 0368 Atmospheric Composition and Structure: Troposphere—constituent transport and chemistry; 0394 Atmospheric Composition and Structure: Instruments and techniques; 1640 Global Change: Remote sensing; *KEYWORDS:* remote sensing, troposphere, error characterization

Citation: Worden, J., S. S. Kulawik, M. W. Shephard, S. A. Clough, H. Worden, K. Bowman, and A. Goldman (2004), Predicted errors of tropospheric emission spectrometer nadir retrievals from spectral window selection, *J. Geophys. Res.*, 109, D09308, doi:10.1029/2004JD004522.

1. Introduction

[2] The Tropospheric Emission Spectrometer [Beer *et al.*, 2001] is one of four instruments on the EOS-Aura platform designed to study the Earth's ozone, air quality, and climate. The TES is an infrared Fourier transform spectrometer (FTS), which measures the spectral infrared (IR) radiances between 650 cm⁻¹ and 3050 cm⁻¹ in a limb-viewing and a nadir (downward looking) mode. The observed IR radiance is imaged onto an array of 16 detectors, which have a combined horizontal footprint of 5.3 km, by 8.4 km in the nadir viewing mode. In the nadir view, TES retrievals will be sensitive to the more abundant tropospheric species such as H₂O, O₃, CO and CH₄. However, because vertical information about trace gas concentrations is obtained only from spectral variations along the line of sight, sufficient spectral resolution and signal-to-noise ratio are required to

distinguish between stratospheric and tropospheric infrared signatures. TES spectral resolution was chosen to match the average pressure-broadened widths of weak infrared molecular transitions in the lower troposphere for nadir measurements (0.1 cm⁻¹ apodized) [Beer *et al.*, 2001]. This paper focuses on the selection of spectral windows to be used for TES nadir retrievals. A future manuscript will describe the spectral window selection for TES limb retrievals.

[3] Spectral windows are desired in order to optimize the quality of a retrieval in part by reducing the effects of known systematic errors on the retrieval as well as by choosing those spectral regions with the best sensitivity to the atmospheric species of interest. Spectral windows are also selected to reduce computational burden without significantly degrading the quality of a retrieval. Error characterization is a necessary part of the spectral window selection when the computed information content is used as the metric for window selection [Rodgers, 1998; Dudhia *et al.*, 2002]. For example, von Clarmann and Echle [1998] and Echle *et al.* [2000] have used information content as a metric for selecting spectral windows, principally for the Michelson Interferometer for Passive Atmospheric Sounding (MIPAS) instrument. Similarly, Chédin *et al.* [2003] describes the selection of channels for the retrieval of CO₂ profiles by computing the infor-

¹Jet Propulsion Laboratory, California Institute of Technology, Pasadena, California, USA.

²Atmospheric and Environmental Research, Inc., Lexington, Massachusetts, USA.

³Department of Physics, University of Denver, Denver, Colorado, USA.

mation content over the Atmospheric InfraRed Sounder (AIRS) channels.

[4] Errors that are considered for the TES spectral window selection are (1) smoothing error that is due to the regularization of a retrieval, (2) measurement error that is due to data noise, (3) systematic errors that are due to uncertainties of surface and atmospheric temperature, retrieved and nonretrieved interfering species and errors due to spectroscopic line parameters, and (4) “cross-state” error that is due to retrieving surface emissivity jointly with the atmospheric parameters of interest. The effects of clouds on TES atmospheric retrievals are not considered in this paper as an error source. Therefore the error covariances reported in this paper are for cloud-free scenes. However, the TES retrieval algorithm will account for the effects of clouds that are uniform across the TES field-of-view by joint retrieval of cloud properties with retrieval of atmospheric trace gas concentrations and temperature. Calibration errors are also not considered because they are unknown at this time. As a result of the spectral window selection and estimation of TES errors we report the expected resolution, accuracy, and precision of TES nadir retrievals for surface and atmospheric temperature, H₂O, O₃, CO, and CH₄ for climatological conditions representative of tropical, polar, and middle latitudes. These a posteriori error covariances also show the altitude domains where these retrievals are sensitive to temperature and trace gas concentrations.

2. TES Noise Equivalent Spectral Radiance

[5] Calibration measurements of the TES have been recorded during thermal vacuum testing to characterize radiometric, spectral and spatial performance. Spectral resolution and the instrument line shape (ILS) were determined from both low-pressure gas cell measurements as well as monochromatic CO₂ laser measurements. Radiometric performance was evaluated using measured spectra of known external radiometric sources and by calibrating these spectra using the measured spectrum from the onboard radiometric source.

[6] The noise equivalent spectral radiance (NESR) is the standard deviation of radiance at each spectral point of a calibrated spectrum. The NESR is estimated using the uncalibrated noise level obtained for each target spectrum from the frequency range outside the optical filter band. The radiometric response function, which converts uncalibrated data numbers to radiance units (watts cm⁻² sr⁻¹/cm⁻¹), is applied to the “out-of-band” noise to obtain the NESR estimate. This single spectrum estimate is verified using an independent calculation that relies on the availability of several spectra measured from the same source in order to provide a statistical sample radiance in order to determine the NESR.

[7] The estimated NESR from calibration measurements is also compared to the predicted NESR from a TES radiometric model. In the case of the TES thermal vacuum measurements, variable signal throughput was observed due to time-dependent parameters such as water ice buildup on the detectors. The radiometric model was adjusted to account for these factors when comparing measured and modeled NESR. Figure 1 shows the expected NESR for a clear-sky nadir view of a tropical atmosphere with a surface temperature around 300 K. The NESRs shown in Figure 1

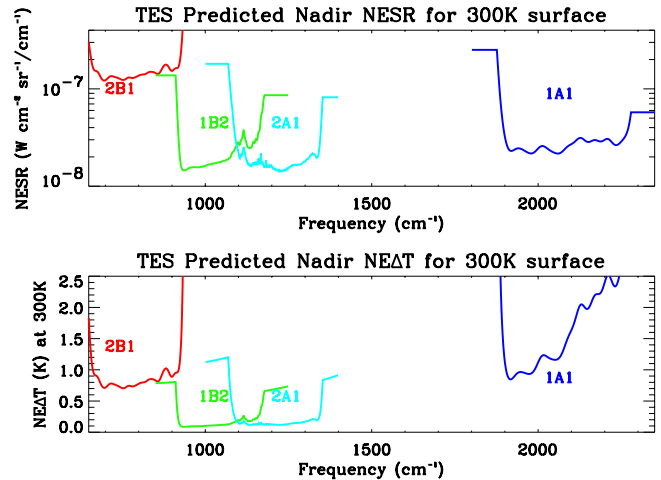


Figure 1. Modeled noise equivalent spectral radiance (NESR) expected for clear-sky nadir observations with a surface temperature of 300 K: (top) radiance units and (bottom) effective brightness temperature difference for the NESR from the top panel. The different colored lines are for the four Tropospheric Emission Spectrometer (TES) filters used for making nadir observations.

are the standard deviation for the measurement error covariance that is used for the spectral window selection and retrieval characterization.

3. Estimation Theory

[8] A spectral window is selected if it increases the information content for a specified set of retrieval parameters (i.e., set of parameters to be inferred with the measurement). The information content depends on the a priori and the a posteriori covariances of the retrieved parameters. The a posteriori covariance depends on measurement error, systematic errors, and the choice of regularization used in the retrieval. In this section we describe the estimation theory and retrieval approach used for performing and characterizing the errors of TES atmospheric retrievals. We then describe how the information content of a retrieval is computed for a selected spectral window.

[9] Measured radiances can be related to a forward model through the following additive noise model:

$$\mathbf{y} = \mathbf{F}(\mathbf{x}, \mathbf{b}; \nu) + \mathbf{n} \quad (1)$$

where $\mathbf{y} \in \mathbb{R}^M$ is the observation vector containing the calibrated, measured spectra. The observation vector is the sum of the nonlinear forward model operator, $\mathbf{F}: \mathbb{R}^N \rightarrow \mathbb{R}^M$, which simulates the radiance produced from the terrestrial surface and atmosphere and observed by the spacecraft. The noise term $\mathbf{n} \in \mathbb{R}^M$ is assumed to be zero-mean, white Gaussian noise so that:

$$\mathbf{S}_n = E[\mathbf{nn}^T] = \sigma^2 \mathbf{I} \quad (2)$$

where $E[\cdot]$ is the expectation operator [Papoulis, 1984], σ is the NESR, and \mathbf{I} is the identity matrix. The forward model

is a function of the “full” state vector, $\mathbf{x} \in \mathbb{R}^N$ where \mathbf{x} can, for example, be the distribution of atmospheric gas, atmospheric temperature, surface temperature, or surface emissivity. The vector \mathbf{b} contains all the other parameters, trace gases, atmospheric temperature distribution, geometry of the measurement, etc., necessary to define the radiance for the TES sensors; these parameters are fixed for any given retrieval.

[10] Operationally, the TES radiances are apodized to reduce systematic errors from the instrument line shape and also reduce computational burden. Apodization introduces correlations between radiance points; however, for simplicity we do not include these correlations in the measurement error covariance described by equation (2).

[11] Fine discretization of the atmosphere is required to model accurately the radiative transfer through the atmosphere. The atmospheric grid used by the TES forward model algorithm contains 87 pressure levels between 1211.53 hPa and 0.1 hPa. However, variations in temperature or trace gas concentrations cannot typically be resolved on this fine vertical grid and therefore the retrieval must be regularized. Regularization of the retrieval includes defining a retrieval vector that limits the possible values of the full state vector. For this study, the retrieval vector and the full state vector are related by a linear mapping:

$$\mathbf{x} = \mathbf{M}\mathbf{z} \quad (3)$$

where \mathbf{z} is the retrieval vector and \mathbf{M} is a mapping matrix. The mapping matrix may also be interpreted as

$$\mathbf{M} = \frac{\partial \mathbf{x}}{\partial \mathbf{z}}. \quad (4)$$

The mapping matrix represents a “hard constraint” because the estimate cannot take on values outside the range space of \mathbf{M} [Rodgers, 2000; Bowman *et al.*, 2002]. Note, maps that have correlations between different types of retrieval parameters are not generated. For example, if the retrieval vector contains both atmospheric water and temperature (or other gas), then the relationship between the full-state vector and retrieval vector is

$$\mathbf{x} = \begin{bmatrix} \mathbf{x}_{H_2O} \\ \mathbf{x}_{TATM} \end{bmatrix} = \begin{pmatrix} \mathbf{M}_{H_2O} & 0 \\ 0 & \mathbf{M}_{TATM} \end{pmatrix} \begin{bmatrix} \mathbf{z}_{H_2O} \\ \mathbf{z}_{TATM} \end{bmatrix} \quad (5)$$

where \mathbf{M}_{H_2O} and \mathbf{M}_{TATM} are the maps for water and temperature, respectively. The elements of water state vector are defined as $[\mathbf{x}_{H_2O}]_i = \ln q(P_i)$ where q is the volume mixing ratio of a P_i pressure scale.

[12] TES operational retrievals will be reported on the full-state pressure grid and therefore the error analysis described in subsequent sections explicitly accounts for mapping between the retrieval levels and this full-state grid. However, for numerical reasons associated with computing the determinant of large matrices, we actually compute the covariance matrices used for the spectral window selection on the retrieval grid. This approximation for computing the error covariances is reasonable if the set of retrieval parameters sufficiently describes the vertical variations of the profile.

3.1. Linear Retrieval

[13] A retrieval can be described by the minimization of the following maximum a posteriori cost function [Tarantola, 1987; Rodgers, 2000]:

$$\hat{\mathbf{x}} = \mathbf{M} \cdot \min_{\mathbf{z}} \left(\|\mathbf{y} - \mathbf{F}(\mathbf{M}\mathbf{z})\|_{\mathbf{S}_n}^2 + \|\mathbf{z} - \mathbf{z}_c\|_{\mathbf{\Lambda}}^2 \right) \quad (6)$$

where \mathbf{z}_c is a constraint vector, $\mathbf{\Lambda}$ is a constraint matrix, and \mathbf{S}_n is the error covariance matrix defined in equation (2). This cost function is optimal when the state vector and measurement error are multivariate normal distributions. The constraint vector and matrix are referred to as “soft” constraints because they provide a priori information about the solution space (e.g., smoothness of the profile or statistical distribution of the state vector), without restricting that solution space for the estimate. The nonlinear retrieval is performed through iterative minimization of the observed radiances with the forward model calculation evaluated at successive estimates of the retrieval vector.

[14] If the estimate is “close” to the true state, then its dependence on the choice of constraint vector, constraint matrix, and true state can be described by the linear retrieval [Rodgers, 2000]:

$$\hat{\mathbf{x}} = \mathbf{x}_c + \mathbf{A}_{xx}(\mathbf{x} - \mathbf{x}_c) + \mathbf{M}\mathbf{G}_z\mathbf{n} + \sum_i \mathbf{M}\mathbf{G}_z\mathbf{K}_b^i(\mathbf{b}^i - \mathbf{b}_a^i) \quad (7)$$

where \mathbf{M} is the mapping matrix, \mathbf{n} is the noise vector, \mathbf{x} is the true full state vector, and $\mathbf{x}_c = \mathbf{M}\mathbf{z}_c$ is the a priori state vector. The vector \mathbf{b} is the true state for those parameters that also affect the modeled radiance, e.g., concentrations of interfering gases, calibration, etc. The vector \mathbf{b}_a is the corresponding a priori values for the vector \mathbf{b} . The Jacobian, $\mathbf{K}_b = \frac{\partial \mathbf{F}}{\partial \mathbf{b}}$, describes the dependency of the forward model radiance, \mathbf{F} , on the vector \mathbf{b} . \mathbf{G}_z is the gain matrix which is defined by

$$\mathbf{G}_z = \frac{\partial \mathbf{z}}{\partial \mathbf{F}} = (\mathbf{K}_z^T \mathbf{S}_n^{-1} \mathbf{K}_z + \mathbf{\Lambda}_z)^{-1} \mathbf{K}_z^T \mathbf{S}_n^{-1}. \quad (8)$$

The retrieval Jacobian, \mathbf{K}_z , is defined by

$$\mathbf{K}_z = \frac{\partial \mathbf{F}}{\partial \mathbf{x}} \frac{\partial \mathbf{x}}{\partial \mathbf{z}} = \mathbf{K}_x \mathbf{M}. \quad (9)$$

Equation (7) is a valid approximation to equation (6) when the estimate is close to the true state, that is,

$$\mathbf{K}_x[\mathbf{x} - \hat{\mathbf{x}}] \approx \mathbf{F}(\mathbf{x}, \mathbf{b}) - \mathbf{F}(\hat{\mathbf{x}}, \mathbf{b}) \quad (10)$$

The averaging kernel matrix or resolution matrix, $\mathbf{A}_{xx} = \frac{\partial \hat{\mathbf{x}}}{\partial \mathbf{x}}$ is the sensitivity of the retrieval to the true state of the atmosphere and is computed by the following equation:

$$\mathbf{A}_{xx} = \frac{\partial \hat{\mathbf{x}}}{\partial \mathbf{x}} = \frac{\partial \hat{\mathbf{x}}}{\partial \mathbf{z}} \frac{\partial \mathbf{z}}{\partial \mathbf{F}} \frac{\partial \mathbf{F}}{\partial \mathbf{x}} = \mathbf{M}\mathbf{G}_z\mathbf{K}_x, \quad (11)$$

The averaging kernel matrix is used to define the “resolution” of the retrieval. The vertical resolution of an atmospheric retrieval, defined on a pressure (or altitude grid), can be derived from the rows of the averaging kernel matrix, $\partial \hat{\mathbf{x}}_i / \partial \mathbf{x}$, which define the relative contribution of each element of the true state to the estimate at a particular pressure (or altitude). The resolution can be defined as the

full width half maximum of the rows of the averaging kernel.

[15] The averaging kernel matrix is also used to compute the DOF for signal of the retrieval [Rodgers, 2000], which is defined as

$$\text{dofs} = \text{tr}[\mathbf{A}_{xx}]. \quad (12)$$

The degrees of freedom for signal of the retrieval may be interpreted as the number of statistically independent elements of the estimate.

3.2. Error Analysis and Information Content

[16] The error in the estimate is the true state minus the estimate:

$$\tilde{\mathbf{x}} = \mathbf{x} - \hat{\mathbf{x}} \quad (13)$$

Substituting equation (7) into equation (13) leads to

$$\tilde{\mathbf{x}} = \underbrace{(\mathbf{I} - \mathbf{A}_{xx})(\mathbf{x} - \mathbf{x}_c)}_{\text{smoothing error}} + \underbrace{\mathbf{M}\mathbf{G}_z\mathbf{n}}_{\text{measurement error}} + \underbrace{\sum_i \mathbf{M}\mathbf{G}_z\mathbf{K}_b^i(\mathbf{b}^i - \mathbf{b}_a^i)}_{\text{systematic errors}}. \quad (14)$$

The right-hand side of this equation is composed of three terms. The first term results from applying constraints to the estimate of retrieval parameter on a specific grid. These constraints can be a combination of “hard” constraints (e.g., representing the profile on a coarse pressure grid) or “soft” constraints (e.g., adding a quadratic penalty function to equation (8)) in order to ensure an acceptable regularization. This first term is the so-called “smoothing” error [Rodgers, 2000]. Physically, the smoothing error describes the uncertainty due to unresolved fine structure. The second term (measurement error) transforms the random instrument spectral error to an error on the full state vector. The third term transforms errors from forward model parameters to an error on the full state vector, for brevity we describe these terms as systematic errors, although some of the errors such as temperature and water can change with each retrieval.

[17] The mean of the error vector defined on the full-state grid (i.e., the grid chosen for the full-state vector) is

$$E[\tilde{\mathbf{x}}] = (\mathbf{I} - \mathbf{A}_{xx})(\mathbf{x} - \mathbf{x}_c), \quad (15)$$

where $\bar{\mathbf{x}} = E[\mathbf{x}]$. Equation (15) is also the mean of the smoothing error and hence represents the bias introduced by the constraint vector and constraint matrix. In the case where the constraint vector is equal to the mean of the “true” state, then the estimate is unbiased. We have assumed a zero-mean measurement noise vector and systematic error for equation (14). The total error covariance matrix after a measurement has been performed is

$$\mathbf{S}_{\tilde{\mathbf{x}}} = (\mathbf{A}_{xx} - \mathbf{I})\mathbf{S}_a(\mathbf{A}_{xx} - \mathbf{I})^T + \mathbf{M}\mathbf{G}_z\mathbf{S}_n\mathbf{G}_z^T\mathbf{M}^T + \sum_i \mathbf{M}\mathbf{G}_z\mathbf{K}_b^i\mathbf{S}_b^i(\mathbf{M}\mathbf{G}_z\mathbf{K}_b^i)^T, \quad (16)$$

where $\mathbf{S}_{\tilde{\mathbf{x}}} = E[(\tilde{\mathbf{x}} - \bar{\tilde{\mathbf{x}}})(\tilde{\mathbf{x}} - \bar{\tilde{\mathbf{x}}})^T]$, $\bar{\tilde{\mathbf{x}}} = E[\tilde{\mathbf{x}}]$, $\mathbf{S}_a = E[(\mathbf{x} - \bar{\mathbf{x}})(\mathbf{x} - \bar{\mathbf{x}})^T]$, and $\mathbf{S}_b = E[(\mathbf{b} - \bar{\mathbf{b}})(\mathbf{b} - \bar{\mathbf{b}})^T]$. The smoothing error

covariance matrix is composed of the averaging kernel and the covariance of the state vector. Hence the smoothing error will decrease as the resolution of the retrieval increases, i.e., the averaging kernel will approximate the identity matrix.

3.3. Cross-State Error

[18] The surface emissivity strongly affects the nadir-viewed radiances; consequently, uncertainties in the surface emissivity degrade the accuracy of TES nadir atmospheric retrievals. There are two approaches we could use to reduce the effect of surface emissivity uncertainties on TES retrievals: (1) retrieve surface emissivity separately and characterize the emissivity error as a systematic error in the retrieval error covariance calculation shown in equation (16) or (2) retrieve surface emissivity jointly with the other atmospheric parameters. We find that retrieving surface emissivity separately introduces unacceptable systematic error into TES atmospheric retrievals. We therefore retrieve emissivity jointly with the atmospheric parameters but compute the information content only over the atmospheric parameters of interest. Retrieving emissivity jointly with the atmospheric parameters of interest has the following effect on the estimate of the atmospheric parameters (noise and systematic error terms are not shown for brevity):

$$\hat{\mathbf{x}} = \mathbf{x}_a + \mathbf{A}_{xx}(\mathbf{x} - \mathbf{x}_a) + \mathbf{A}_{x\varepsilon}(\varepsilon - \varepsilon_a), \quad (17)$$

where the matrix \mathbf{A} refers to the full averaging kernel for the joint retrieval, the vector “ \mathbf{x} ” refers to the atmospheric parameters of interest, and the vector “ ε ” refers to the set of emissivity parameters. Therefore \mathbf{A}_{xx} refers to the submatrix of \mathbf{A} that is associated with the vector \mathbf{x} , and $\mathbf{A}_{x\varepsilon}$ refers to the submatrix of \mathbf{A} that relates the sensitivity of the vector \mathbf{x} to the vector of emissivities. The a posteriori error covariance (now including noise and systematic errors) for the estimate of $\hat{\mathbf{x}}$ is

$$\mathbf{S}_{\hat{\mathbf{x}}} = (\mathbf{A}_{xx} - \mathbf{I})\mathbf{S}_a(\mathbf{A}_{xx} - \mathbf{I})^T + (\mathbf{A}_{x\varepsilon})\mathbf{S}_a^{\varepsilon\varepsilon}(\mathbf{A}_{x\varepsilon})^T + \mathbf{M}\mathbf{G}_z\mathbf{S}_n\mathbf{G}_z^T\mathbf{M}^T + \sum_i \mathbf{M}\mathbf{G}_z\mathbf{K}_b^i\mathbf{S}_b^i(\mathbf{M}\mathbf{G}_z\mathbf{K}_b^i)^T \quad (18)$$

where \mathbf{S}_a refers to the a priori covariance for the atmospheric parameters of interest (i.e., the vector \mathbf{x}) and $\mathbf{S}_a^{\varepsilon\varepsilon}$ is the a priori covariance for emissivity. The gain matrix and Jacobians in equation (18) do not include the emissivity parameters. The first term in this equation is the smoothing error; the second term is what we have defined as the “cross-state” error because it is the error of the estimate for the parameters of interest (e.g., the atmospheric parameters) due to jointly retrieving with an additional set of parameters (e.g., emissivity). We note that the covariance, $\mathbf{S}_{\hat{\mathbf{x}}}$, in equation (18) for the vector \mathbf{x} is equivalent to the submatrix of the total error covariance for the joint retrieval which corresponds to the atmospheric parameters.

3.4. Information Content

[19] A measure of the performance of the retrieval is the “information content” [Rodgers, 2000], which is defined as

$$\Delta\mathbf{H} = \frac{1}{2} \log_2 \left(\frac{|\mathbf{S}_a|}{|\mathbf{S}_{\hat{\mathbf{x}}}|} \right) = \frac{1}{2} (\log_2 |\mathbf{S}_a| - \log_2 |\mathbf{S}_{\hat{\mathbf{x}}}|), \quad (19)$$

where $||$ is the determinant operator. The determinant of the total error covariance matrix defines the total error volume for the covariance. Therefore the information content describes the decrease in error volume relative to the error volume calculated from the a priori covariance matrix of the atmospheric state. The unit of information content in equation (19) is bits. The information content increases by one bit for every factor of 2 decrease in error volume relative to the volume of uncertainty of the atmospheric state.

4. Spectral Windows Selection Approach

[20] Spectral windows are chosen to be the same for all nadir observations in order to ensure that biases from line parameters associated with using scene-dependent spectral windows are not introduced into TES retrievals. Consequently, we select a set of spectral windows that maximize the combined information content of four regions representative of different climatological conditions: northern mid-latitude, southern midlatitude, tropical, and polar. A priori covariances are generated for each region using the Model for Ozone and Related Chemical Tracers (MOZART) [Brasseur *et al.*, 1998]. Spectral windows that increase the total information content of the sum all four regions are then selected,

$$\Delta \mathbf{H}_{total} = \sum_i \Delta \mathbf{H}_i, \quad (20)$$

where the index, i , indicates one of the four regions.

[21] Spectral windows are also chosen to reflect a particular retrieval sequence. Surface temperature, atmospheric temperature, and water vapor affect the atmospheric equation of state and consequently the retrieval of all atmospheric species observed by TES. Therefore spectral windows that maximize the information content of a joint retrieval of these parameters are selected first. The joint a posteriori error covariance of surface temperature, atmospheric temperature, and water is propagated as a systematic error for selecting spectral windows for ozone, methane, and carbon monoxide. Note that the full joint error covariance, with cross correlations between temperature and water terms, is propagated as a systematic error. Ignoring the cross correlations can increase the error volume (or decrease the information content) of this joint retrieval and hence can significantly affect the spectral window selection for retrievals of trace gas concentrations. Spectral windows for ozone were selected next with the resulting error covariance used as a systematic error in the spectral window selection for methane and carbon monoxide.

[22] The procedure used for selecting for TES nadir spectral windows is the following:

[23] 1. Calculate information content for a small window that is scanned across the spectral range of the appropriate TES filter. Our window size for scanning was chosen to be (an ad hoc) four spectral points (0.24 cm^{-1}).

[24] 2. Select window with the largest information content and expand window by four points on alternate sides. The expanded windows are evaluated using a sequential update approach [e.g., Rodgers, 2000; Dudhia *et al.*, 2002] in order to reduce computation time. If the a posteriori error

from the expanded window results in positive information content then the window is selected and again expanded. This process is repeated until the a posteriori error decreases the information content. If the spectral window expansion decreases the information content the new addition is ignored, the spectral range of the window is recorded, and the a priori covariance is replaced by the a posteriori covariance in order to evaluate the next window.

[25] 3. Steps 1 and 2 are repeated until either a desired number of unique windows are found or there is no positive increase in information content left in the spectral regions remaining across the filter.

[26] We applied additional selection criteria and modifications to the selected spectral windows after the automated process described by steps 1 through 3 in order to reduce the computation burden of a retrieval and ensure that each window contributes positively with the final ensemble of windows. For example, after all the spectral windows are selected they are sorted by information content. Windows that contributed only a small amount of information content were discarded. It is also possible that some windows contribute positive information content against the original a priori covariance but negative information content against an updated a priori covariance. Therefore we sometimes found windows that showed negative information content after this final sorting process; these windows were also discarded. Windows that were spectrally “close,” that is, within the spectral half width of the instrument line shape, were combined if the incurred negative change in information content was minimal.

5. Spectral-Window Selection for Surface Temperature, Atmospheric Temperature, and H₂O

[27] Spectral windows for the retrieval of surface temperature, atmospheric temperature, and water vapor are selected using spectral sensitivities calculated within the band passes of the TES 2B1 (650 cm^{-1} – 900 cm^{-1}) and 2A1 (1100 cm^{-1} – 1320 cm^{-1}) filters. The 2B1 spectral band pass encompasses the $15 \text{ }\mu\text{m}$ CO₂ band as well as a “window” region near 900 cm^{-1} where there is little atmospheric absorption. The spectral band pass of the 2A1 filter includes several water absorption lines, the $7.8 \text{ }\mu\text{m}$ CH₄ band, and several window regions with little atmospheric absorption.

[28] A priori covariances for temperature and H₂O are constructed by first generating a climatological covariance using one day from a run of the MOZART model [Brasseur *et al.*, 1998]. However, the climatological variances are larger than the expected uncertainty from predictions of atmospheric temperature and water vapor from the National Center for Environmental Prediction (NCEP) (e.g., see <http://www.ncep.noaa.gov/>), which will be used as a priori for TES retrievals. Because we were only able to obtain standard deviations of uncertainties at coarse pressure resolution from NCEP, we chose to scale MOZART climatologies to the NCEP standard deviations.

[29] We choose the constraint matrix to be the inverse of the a priori covariance. The a priori covariance for emissivity assumes a standard deviation of 0.1 with no correlations between emissivity parameters. This standard deviation is based upon examining land surface emissivity

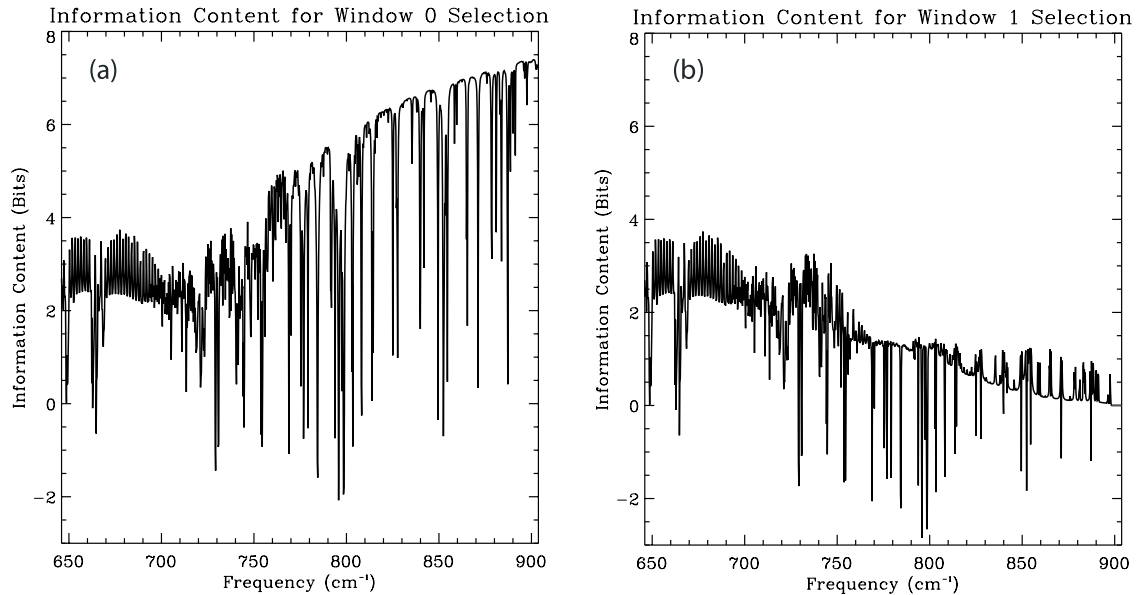


Figure 2. (a) Information content across the TES 2B1 filter before any spectral window is selected. The filter is divided into a set of 0.24 cm^{-1} windows, and the information content is computed for each window. (b) Information content across the TES 2B1 filter after the first spectral window is selected.

variability from the ASTER [Yamaguchi *et al.*, 1998] database for this spectral region. The covariance for the measurement noise is diagonal and is the inverse square of the NESR discussed in section 2.

[30] Jacobians are computed analytically for both the retrieved parameters and interferents using the TES forward model algorithm [e.g., Clough and Iacono, 1995; Clough *et al.*, 2004; Worden *et al.*, 2004], which is based on the Line By Line Radiative Transfer Model (LBLRTM) [e.g., Clough and Iacono, 1995; Clough *et al.*, 2004]. Trace gas interferents for the 2B1 filter are assumed to be O_3 and H_2O . Trace gas interferents assumed for the 2A1 filter are N_2O , CH_4 , O_3 , and the water isotope HDO. Covariances for these trace gases are generated using MOZART. Line parameter errors are also included for these retrieved and interfering trace gases (Appendix A).

[31] The strategy for performing a retrieval of surface temperature, atmospheric temperature, and water is (1) perform an initial retrieval of surface temperature and atmospheric temperature using only the 2B1 filter and (2) perform a retrieval of surface temperature, atmospheric temperature, and water using the updated surface temperature and atmospheric temperature from step 1 and radiances from both the 2B1 and 2A1 filters. This strategy is utilized to reduce the possibility that a retrieval will jump into a local minimum that is nonphysical. Our spectral window selection also follows this strategy; that is, spectral windows are first selected for a retrieval of surface and atmospheric temperature using the 2B1 filter. Spectral windows are then selected for a joint retrieval of surface temperature, atmospheric temperature, and H_2O using only the 2A1 filter. Note that the a posteriori covariance from the 2B1 filter spectral window selection is used as part of the a priori covariance for the 2A1 spectral window selection.

[32] Figures 2a and 2b show the information content across the TES 2B1 filter used to start the spectral window

selections for the atmospheric and surface temperature retrievals. Figure 2a shows that for the first pass across the 2B1 filter, the information content peaks in the “window” spectral region where there is little atmospheric absorption. Consequently, the first spectral window will reduce the uncertainty associated with surface temperature. Figure 2b shows the information content across the 2B1 filter after the first window is chosen. The information content now peaks in the CO_2 band; selection of spectral windows in the CO_2 band primarily reduces the a priori error associated with atmospheric temperature.

[33] The top panels of Figure 3a and Figure 3b shows the computed radiance for the TES 2B1 and 2A1 filters for the northern midlatitude profile. The selected spectral windows for the retrieval of atmospheric and surface temperature and H_2O are shown overlying the radiances in the top panels of Figures 3a and 3b, respectively. The middle and bottom panels of Figures 3a and 3b show the estimated radiance error from the interferents and line parameter errors, respectively; the radiance error is computed with the following equation:

$$|\delta L_\nu| \approx (\mathbf{K}_b \mathbf{S}_b \mathbf{K}_b^T)_{\nu\nu}^{1/2} \quad (21)$$

where δL_ν is the radiance error, the index ν refers to the frequency index, \mathbf{K}_b is the Jacobian for systematic error b , and \mathbf{S}_b is the error covariance matrix. The species that contributes the most to the estimated radiance error at each spectral point is also shown. For comparison, the NESR for each filter is shown as a dotted line in the middle panel. The bottom panel of Figures 3a and 3b shows the radiance error estimated from the line parameter uncertainties in these spectral regions (Appendix A). The estimated radiance errors indicate spectral regions that are likely to be selected. For example, the spectral windows shown for the 2A1 filter

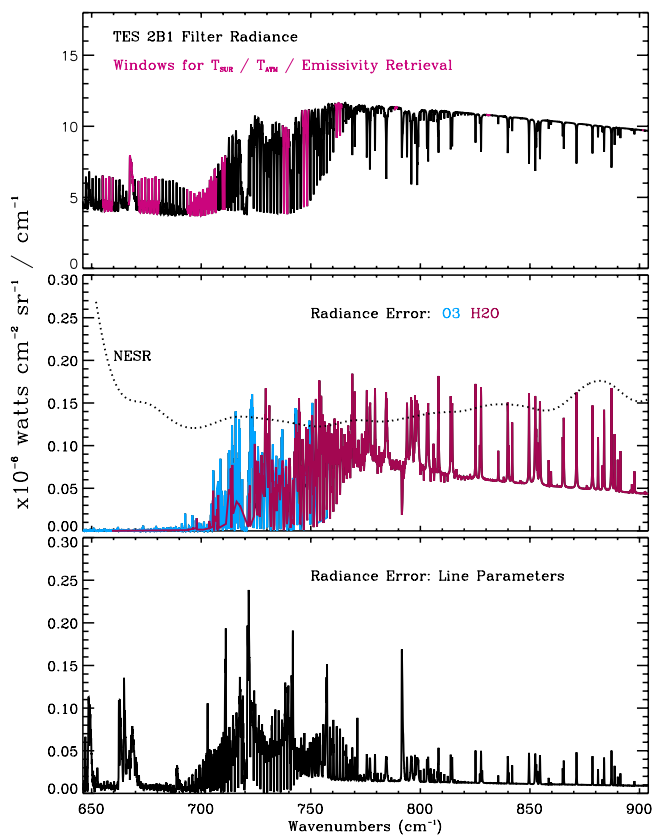


Figure 3a. (top) Computed radiance for the TES 2B1 filter for the northern midlatitude profile. The spectral windows for the retrieval of surface temperature, atmospheric temperature, and H_2O are shown overlying the radiance. (middle) Estimated radiance error from the NESR and spectral interferences (O_3 and H_2O). (bottom) Line parameter errors.

occur where the radiance errors from interferences and line parameters are smaller than those of adjacent spectral regions.

[34] Figures 4a and 4b show error estimates for the retrieval of the northern midlatitude profile of surface temperature, atmospheric temperature, and H_2O , using the final set of spectral windows. For Figures 4a and 4b, the square root of the diagonal values of the a priori covariance are shown as the solid black line with plus and minus values about zero. The diamonds indicate retrieval levels. The square root of the diagonal of the a posteriori error covariance for a retrieval using the selected spectral windows is shown as a dashed line. The dominant error is typically smoothing error. As discussed earlier, smoothing error describes the extent that the retrieval infers fine structure on the reported altitude grid. Consequently, the smoothing error is reduced if the vertical resolution increases. In addition to showing the reduction in error for atmospheric and surface temperature and H_2O , Figures 4a and 4b also indicate the altitude range where the retrieval is most sensitive. For example, the retrieval is sensitive to H_2O concentrations below about 11 km in the northern midlatitude profile and is sensitive to atmospheric temperature from the stratosphere down to the surface.

[35] Tables 1 and 2 show estimated vertical resolutions for specific altitude ranges for the four atmospheric profiles used in the spectral window selection. Average vertical resolutions are computed for the indicated pressure range shown in each table. The vertical resolution at some pressure is computed from the full width at half maximum (FWHM) of the corresponding row of the averaging kernel matrix as discussed in section 3.1. Tables 1 and 2 also show the degrees of freedom (equation (12)) and the reduction in error, as indicated by the number of bits (equation (19)), for the four profiles. In general, arctic regions have fewer degrees of freedom and reduction in uncertainty from the a priori because of the greatly reduced surface temperature and water content as compared to the other regions.

6. Spectral Window Selection for O_3

[36] Spectral windows are selected for ozone retrievals using spectral sensitivities calculated within the band pass of the TES 1B2 filter. This filter spans the spectral range between 950 cm^{-1} and 1150 cm^{-1} , which encompasses the $9.6\text{ }\mu\text{m}$ ozone band. The NESR for the TES 1B2 filter is shown in Figure 1. The climatological covariance for ozone is constructed from the MOZART model, however, this covariance is adjusted to remove correlations between the troposphere and upper stratosphere that are likely unphysical. Systematic errors used for the spectral window selec-

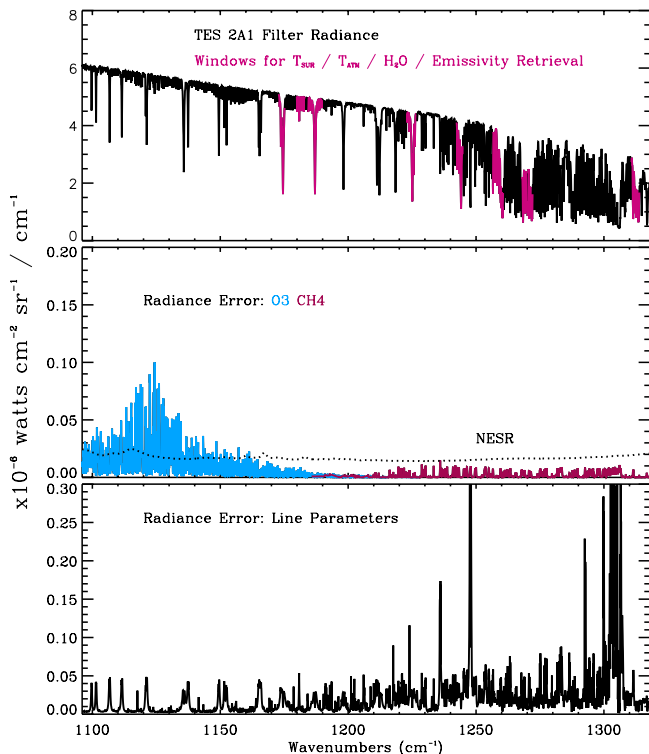


Figure 3b. (top) Computed radiance for the TES 2A1 filter for the northern midlatitude profile. The spectral windows for the retrieval of surface temperature, atmospheric temperature, and H_2O are shown overlying the radiance. (middle) Estimated radiance error from the NESR and spectral interferences (O_3 and CH_4). (bottom) Line parameter errors.

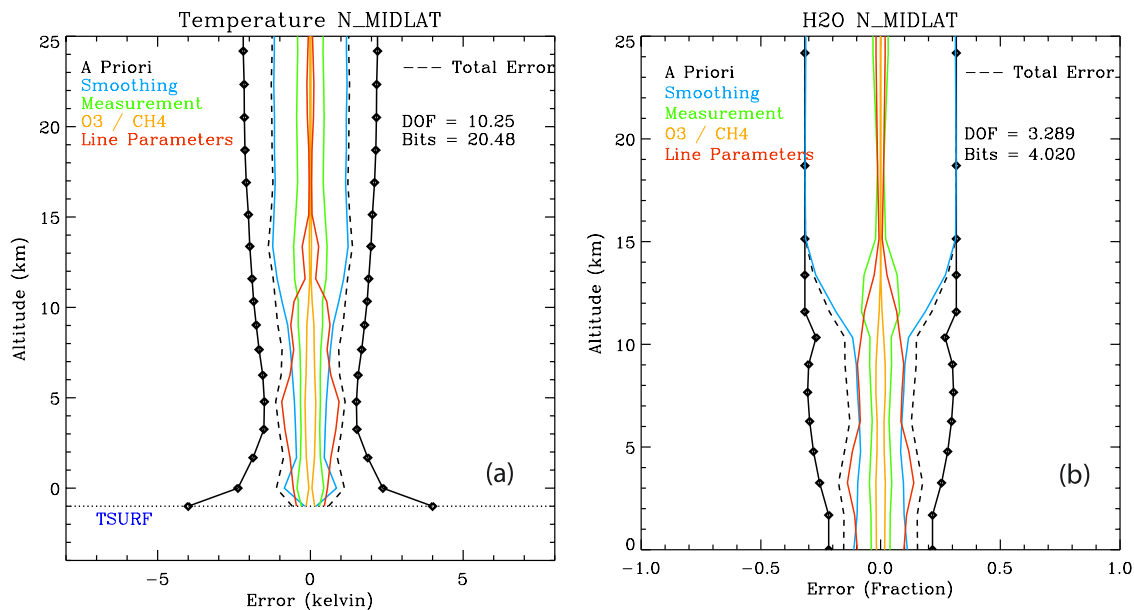


Figure 4. (a) Estimated errors for north midlatitude retrieval of surface and atmospheric temperature. The initial climatological variability is shown with the solid black line, and the final retrieval error is shown with the dashed line. The a posteriori (or total) error is composed of smoothing error (blue), measurement error (green), errors from the spectrally interfering species O₃ and CH₄ (orange), and line parameter errors (red). The cross-state error associated with retrieving H₂O and emissivity jointly with temperature are included into the smoothing error. (b) Estimated errors for the north midlatitude retrieval of H₂O. The initial climatological variability is shown with the solid black line, and the final retrieval error is shown with the dashed line. The final retrieval error is composed of smoothing error (blue), measurement error (green), errors from the spectrally interfering species O₃ and CH₄ (orange), and line parameter errors (red).

tion include (1) estimated errors for spectroscopic parameters of CO₂, O₃, and H₂O and (2) the total error covariance from the surface temperature, atmospheric temperature, and H₂O retrieval discussed in section 4. As previously discussed, emissivity is jointly retrieved with ozone in the spectral window selection process; as with the previous retrieval, the a priori error covariance for the emissivity is assumed to be a diagonal with a standard deviation of 0.1.

[37] The selected spectral windows for the retrieval of ozone are shown in the top panel of Figure 5. The top panel of Figure 5 shows the computed radiance for the TES 1B2 filter for the northern midlatitude profile. The spectral windows are shown overlying the radiances. The second and third panels show the estimated radiance error from the temperature and water uncertainties as well as line

Table 1. Retrieval Characterization for Atmospheric Temperature Retrieval^a

	Northern Midlatitudes	Southern Midlatitudes	Tropics	Polar
1000–400 hPa resolution	2.7 km	4.4 km	2.1 km	6.9 km
400–100 hPa resolution	4.1 km	5.8 km	3.8 km	7.4 km
100–10 hPa resolution	8.0 km	10.0 km	7.6 km	9.9 km
Total DOF	10.3	7.9	10.9	6.3
Total bits	20.1	15.4	19.1	12.1

^aThe first three rows show the average vertical resolution for the indicated pressures. The total DOF refers to the total degrees of freedom, which is the trace of the averaging kernel. The total number of bits indicates the reduction in error volume for the retrieval.

parameter errors. The radiance error was computed using equation (21).

[38] Figure 6 shows the expected error budget for the retrieval of the northern midlatitude profile of ozone using the selected spectral windows. As with Figure 4, the square root of the diagonal values of the a priori covariance are shown as the solid black line with plus and minus values about zero. The diamonds indicate retrieval levels. The square root of the diagonal of the a posteriori error covariance for a retrieval using the selected spectral windows is shown as a dashed line. Table 3 shows estimated vertical resolutions, total number of bits, and degrees of freedom for the four regions used in the spectral window selection. In general, there are about 5 degrees of freedom for the ozone retrieval with about 2.4 degrees of freedom associated with the troposphere.

[39] A study by *Bowman et al.* [2002] also shows that TES ozone retrievals will have about 2 degrees of freedom in the troposphere and that this resolution is sufficient for inferring daily variations of lower and upper tropospheric

Table 2. Retrieval Characterization for H₂O Retrieval

	Northern Midlatitudes	Southern Midlatitudes	Tropics	Polar
1000–400 hPa resolution	4.3 km	4.1 km	4.0 km	6.0 km
400–100 hPa resolution	3.8 km	4.6 km	3.9 km	11.6 km
Total DOF	3.3	3.2	3.4	1.4
Total bits	4.0	4.5	3.9	1.7

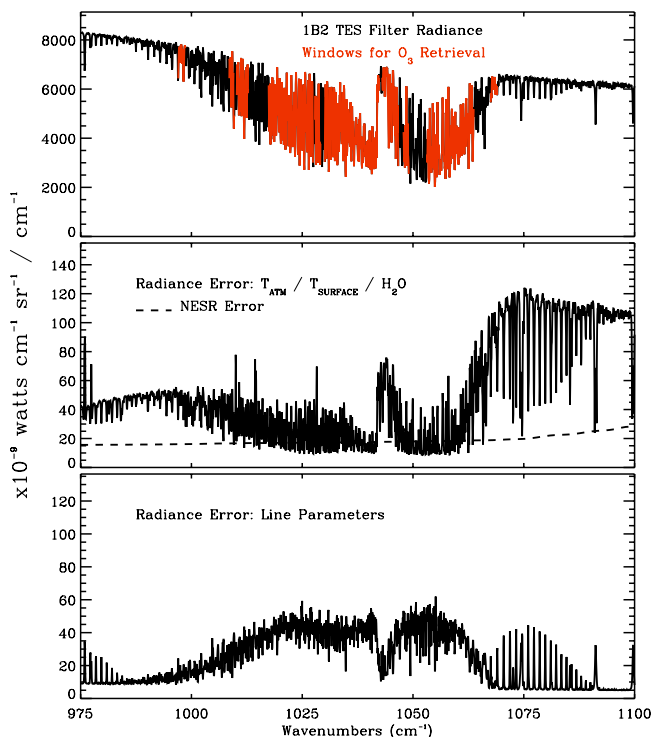


Figure 5. (top) Computed radiance for the TES 1B2 filter for the northern midlatitude profile. The spectral windows for the retrieval of ozone are shown overlying the radiance. (middle) Estimated radiance error due to uncertainties of H_2O and temperature. (bottom) Estimated radiance error from line parameter errors. The NESR for the 1B2 filter is shown in the middle panel.

integrated ozone amounts. The *Bowman et al.* [2002] study shows larger sensitivity of TES ozone retrievals to boundary layer ozone concentrations; this increased sensitivity (as compared to the results reported in this manuscript) results from a more optimistic NESR and a greater thermal contrast between the surface and boundary layer temperatures.

7. CO

[40] Spectral windows are selected for atmospheric carbon monoxide retrievals using spectral sensitivities calculated within the band pass of the TES 1A1 (1890 cm^{-1} – 2260 cm^{-1}) filter. This spectral domain includes $4.7\text{ }\mu\text{m}$ CO band. A priori climatologies for carbon monoxide are generated using MOZART. Systematic errors include the total error covariance from the surface temperature, atmospheric temperature, H_2O and O_3 retrievals discussed in section 4 as well as errors from nonretrieved species such as CH_4 , OCS , and N_2O . (Note that CH_4 is retrieved after CO.) CO line parameter uncertainties were not included as systematic errors as it was decided that line parameter uncertainties in this spectral domain were small enough to ignore.

[41] The top panel of Figure 7 shows the computed radiance for the TES 1A1 filter for the northern midlatitude profile. The selected spectral windows for the retrieval of CO are shown overlying the radiance in the top panel of Figure 7. The middle and bottom panels show the estimated radiance error from the uncertainties in surface temperature,

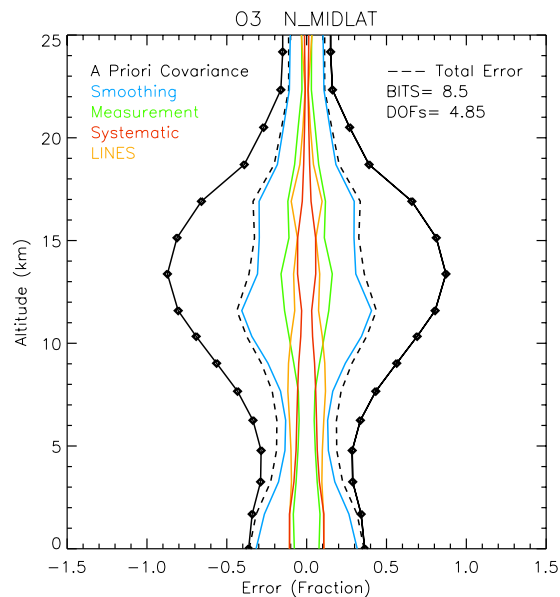


Figure 6. Estimated errors for northern midlatitude O_3 retrieval using selected spectral windows shown in Figure 5. The initial climatological variability is shown with the solid black line, and the a posteriori (total) error is shown with the dashed line. Total error is composed of smoothing error (blue), measurement error (green), systematic errors from H_2O and atmospheric and surface temperature (red), and line parameter errors (orange).

atmospheric temperature, water vapor and other interferences, respectively.

[42] Figure 8 shows the northern midlatitude profile error estimates for the retrieval of carbon monoxide. The retrieval is sensitive to CO concentrations between about 5 km and 15 km. Table 4 shows the total number of bits and DOF for the retrieval of the four atmospheric profiles used for the spectral window selection. There is about 1 degree of freedom for each retrieved profile. Vertical resolutions are not included in Table 4 because there were not enough degrees of freedom to characterize vertical resolutions over several altitude regions.

8. CH_4

[43] Spectral windows are selected for methane retrievals using spectral sensitivities calculated within the band pass of the TES 2A1 (1100 cm^{-1} and 1320 cm^{-1}) filter; this spectral domain includes many H_2O , N_2O , and HDO absorption lines as well as the $7.8\text{ }\mu\text{m}$ CH_4 band. A priori

Table 3. Retrieval Characterization for Ozone Retrieval^a

	Northern Midlatitudes	Southern Midlatitudes	Tropics	Polar
700–400 hPa resolution	6.6 km	6.3 km	6.8 km	5.4 km
400–100 hPa resolution	5.1 km	7.0 km	4.9 km	5.2 km
100–10 hPa resolution	10.2 km	10.4 km	10.3 km	8.7 km
Total DOF	4.9	4.8	4.7	4.6
Total bits	8.5	8.3	6.3	6.3

^aThe first three columns show the average vertical resolution for the indicated pressures. The total DOF refers to the total degrees of freedom, which is the trace of the averaging kernel. The total number of bits indicates the reduction in error volume for the retrieval.

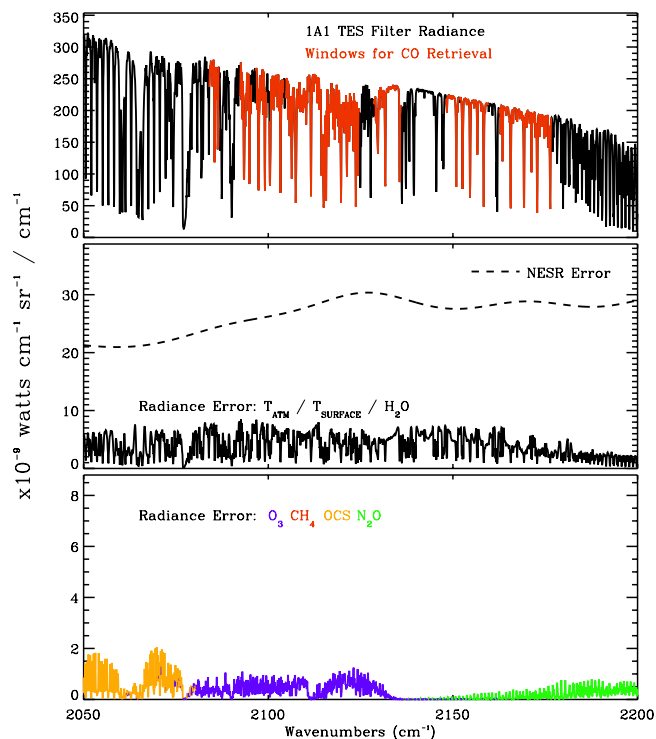


Figure 7. (top) Simulated radiance for the 1A1 filter for the northern midlatitude profile with the final spectral windows for the CO retrieval shown in red. (middle) Estimated radiance error due to uncertainties in temperature and water amounts (from the temperature and water retrieval). The NESR for the 1A1 filter is also shown in the middle panel. (bottom) Estimated radiance errors from spectrally interfering species.

climatologies for methane are generated using MOZART. Systematic errors used by the spectral window selection only include the total error covariance from the surface temperature, atmospheric temperature, and H₂O retrieval discussed in section 4.

8.1. Challenges With Selecting Methane Spectral Windows

[44] A challenging aspect in selecting spectral windows for the TES methane retrievals is that the a priori covariances show little variability in the troposphere; consequently, it is unlikely that TES can reduce the uncertainty associated with tropospheric methane unless there are regions that contain methane amounts that are outside climatological values. Furthermore, no spectral windows are selected when line parameter errors are included with the total estimated error because the computed information content is negative or zero for every spectral point. If line parameter uncertainties are not included as a systematic error, it is found that a single line between 1305.12 cm⁻¹ and 1306.18 cm⁻¹ contains the most information content and other selected lines contain negligible information content; this is a result of the small variability seen in the tropospheric methane climatologies and because the line with the most information content is sensitive to methane in the upper troposphere and stratosphere where methane is expected to have larger climatological variances.

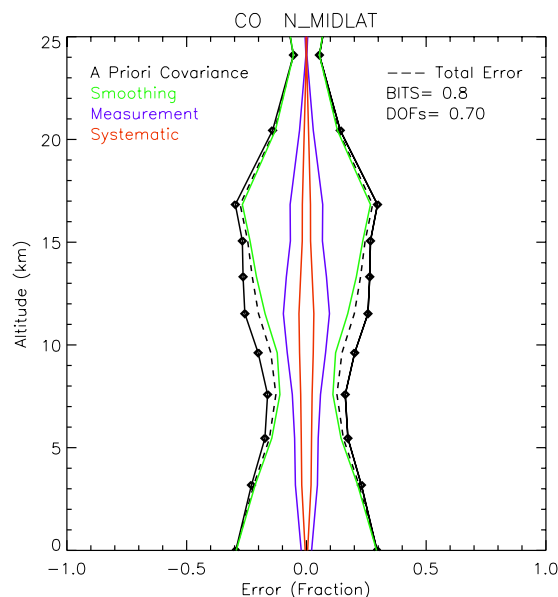


Figure 8. Estimated errors for northern midlatitude CO retrieval using selected spectral windows shown in Figure 7.

[45] The spectral line with the most information content is part of the Q branch. It was therefore decided to only use the Q branch at 1306 cm⁻¹ for the retrieval of methane in order to remove the effects of different systematic biases on the methane retrieval as a result of using lines from the multiple methane branches. Biases associated with the Q branch line can be reduced by comparison of TES retrievals with other measurements. However, it is also thought that unquantified line mixing can affect the radiative absorption for this line [Brown *et al.*, 2003]. It therefore may be necessary to reexamine the TES spectral windows for methane retrievals after TES begins operation.

8.2. Results

[46] Figure 9 shows the northern midlatitude profile error estimates for the retrieval of methane. Table 5 shows the total number of bits and DOF for the four retrieved atmospheric profiles. In general, these retrievals are sensitive to methane concentrations in the upper troposphere and lower stratosphere. There is typically less than 1 degree of freedom and one bit of information content for each retrieval.

9. Summary and Discussion

[47] Spectral windows are defined for Tropospheric Emission Spectrometer (TES) nadir retrievals of surface temperature, atmospheric temperature, H₂O, O₃, CO, and

Table 4. Retrieval Characterization for Carbon Monoxide Retrieval^a

	Northern Midlatitudes	Southern Midlatitudes	Tropics	Polar
Total DOF	0.7	0.8	0.9	0.5
Total bits	0.8	1.1	1.4	0.4

^aEstimated vertical resolutions for carbon monoxide are not shown because there are too few degrees of freedom. However, the simulated TES retrievals are primarily sensitive to CO between approximately 5 and 13 km over the four climatological regions.

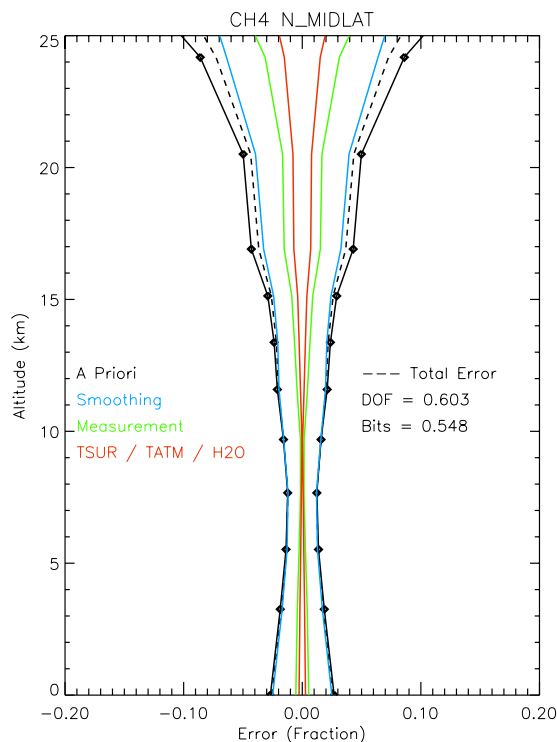


Figure 9. Estimated errors for northern midlatitude CH₄ retrieval. Only a single spectral window between 1305.12 cm⁻¹ and 1306.18 cm⁻¹ is used for this retrieval.

CH₄. In order to ensure that spectral windows are robust over a variety of climatological conditions, spectral windows are selected which maximize the combined information content for retrievals of four regions representative of northern midlatitude, southern midlatitude, tropical, and polar climates. Errors that are considered for the spectral window selection included smoothing error, measurement error, uncertainties with atmospheric temperature and interfering species, and line parameter uncertainties. A cross state error which is due to retrieving emissivity jointly with the atmospheric parameters of interest is also included in the error budget.

[48] The averaging kernels and error covariances from this spectral window selection are used to predict the estimated vertical resolution, information content, accuracy, and precision for the troposphere and lower stratosphere for the four profiles used in the spectral window selection. These metrics for the TES nadir retrievals can be used to assess which atmospheric related questions can be addressed by TES data.

[49] The proper characterization of TES atmospheric retrievals is also critical for applications such as data assimilation and inverse modeling. For example, a study by Jones *et al.* [2003] compared CO fields from the

Table 5. Retrieval Characterization for Methane Retrieval

	Northern Midlatitudes	Southern Midlatitudes	Tropics	Polar
Total DOF	0.60	0.69	0.43	0.65
Total Bits	0.55	0.73	0.30	0.71

GEOS-CHEM model to simulated TES retrievals. The TES averaging kernel matrix and constraint vector were applied to the GEOS-CHEM profiles in order to compare these two sets of CO profiles. This method of comparison accounts for the biases and smoothing from TES retrievals. Jones *et al.* [2003] found that the TES CO retrievals, as characterized in this paper, have enough vertical resolution and accuracy to estimate at least nine globally distributed carbon monoxide sources, which are associated with geopolitical boundaries.

Appendix A: Spectral Line Parameter Uncertainties

[50] The accuracy of the TES atmospheric forward model spectral radiances depends on spectral line parameter uncertainties. Line parameter uncertainties are estimated using the HITRAN [Rothman *et al.*, 1992] database as a guide but also based upon prior comparisons between measured and modeled IR radiances and experience with spectral line measurements. Line parameter uncertainties are primarily dependent on the strength of the line because the line strength determines whether the line parameters are directly measured, or calculated using a physical or statistical model. These uncertainties are mapped to the covariance of retrieved parameters in the following manner:

[51] 1. Estimated uncertainties are computed for the spectroscopic parameters of a species; refer to Table A1 for an example of estimated of H₂O uncertainties.

[52] 2. A reference radiance spectrum is computed.

[53] 3. A line parameter (i.e., a spectral strength, width, or shift) is adjusted for the species for the spectral region of interest by the estimated uncertainty and a new radiance spectrum is computed. The difference between this new radiance and the reference radiance is the estimated radiance error for this spectral line parameter (e.g., Figure A1). Note, that it is computationally intractable at this time to adjust the spectral strength, width, and shifts of individual lines.

[54] 4. Spectral radiance errors are mapped to the covariance of the retrieved parameters using equation (16) except that the columns of the Jacobians are these calculated radiance errors and the covariance; S_b is a matrix in which the diagonal entries have a value of 1. We use this approach for mapping spectral line parameter uncertainties into the retrieved parameter covariances in order to account for correlations between the line parameter uncertainties.

[55] Spectral radiance errors have been computed for four representative atmospheres (northern midlatitude, southern

Table A1. Line Parameter Uncertainties for H₂O Between 1150 cm⁻¹ and 1320 cm^{-1a}

Strength Range at 296 K, ^b cm ⁻¹ (molecule cm ⁻²) ⁻¹	H ₂ O Spectroscopic Error Estimates		
	Strength, %	Widths, %	Shifts, cm ⁻¹
S > 1.0E-21	3	3	1.0E-4
1.0E-21 > S > 1.0E-22	4	4	1.0E-3
1.0E-22 > S > 6.0E-24	7	7	2.0E-3
6.0E-24 > S > 4.0E-26	10	10	5.0E-3
4.0E-26 > S > 1.0E-40	25	25	1.0E-2
S < 1.0E-40	100	100	1.0E-1

^aRead, for example, 1.0E-21 as 1.0×10^{-21} .

^bThe water vapor continuum errors for this spectral region are 4% for the self and 5% for the foreign.

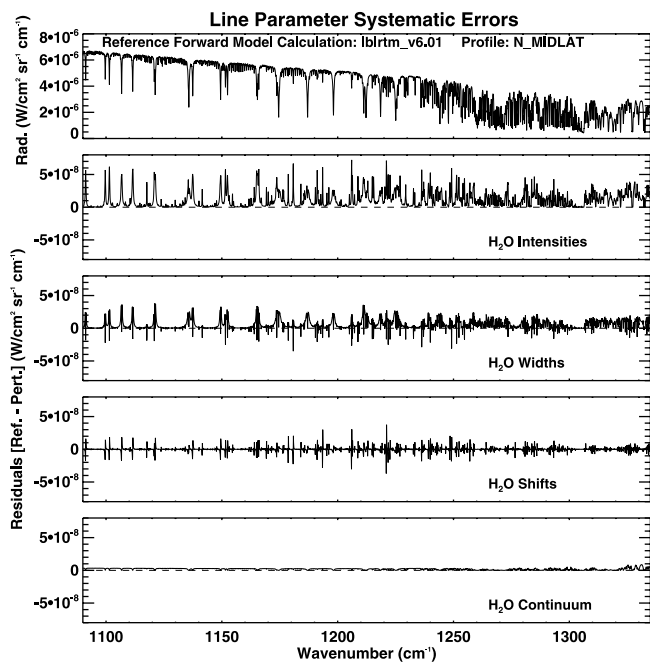


Figure A1. Line parameter systematic errors. Residual radiances are computed and shown in each panel by first computing a reference radiance and then adjusting the indicated H₂O line parameters by the estimated error and recomputing the radiance.

midlatitude, polar, and tropics) and used in the spectral window selection for all the retrieved TES species and primary interferents (e.g., N₂O). Table A1 shows an example of the H₂O line parameter errors for the TES 2A1 filter spectral region.

[56] **Acknowledgments.** We would like to thank Tilman Steck, Linda Brown, Gregory Osterman, Curtis Rinsland, Reinhard Beer, Clive Rodgers, Evan Fishbein, and Michael Gunson for their suggestions, discussions, and contributions to this research. We would also like to thank the two anonymous referees who provided thorough and thoughtful reviews of this manuscript. The research described in this paper was performed at the Jet Propulsion Laboratory, California Institute of Technology, under a contract with the National Aeronautics and Space Administration.

References

- Beer, R., T. A. Glavich, and D. M. Rider (2001), Tropospheric emission spectrometer for the Earth Observing System's Aura Satellite, *Appl. Opt.*, **40**(15), 2356–2367.
- Bowman, K. W., J. Worden, T. Steck, H. M. Worden, S. Clough, and C. Rodgers (2002), Capturing time and vertical variability of tropospheric

ozone: A study using TES nadir retrievals, *J. Geophys. Res.*, **107**(D23), 4723, doi:10.1029/2002JD002150.

Brasseur, G. P., D. A. Hauglustaine, S. Walters, P. J. Rasch, J. F. Muller, C. Granier, and X. X. Tie (1998), MOZART, a global chemical transport model for ozone and related chemical tracers: 1. Model description, *J. Geophys. Res.*, **103**(D21), 28,265–28,289.

Brown, L. R., et al. (2003), Methane line parameters in HITRAN, *J. Quant. Spectrosc. Radiat. Transfer*, **82**(1–4), 219–238.

Chédin, A., R. Saunders, A. Hollingsworth, N. A. Scott, M. Matricardi, J. Etcheto, C. Clerbaux, R. Armante, and C. Crevoisier (2003), The feasibility of monitoring CO₂ from high-resolution infrared sounders, *J. Geophys. Res.*, **108**(D2), 4064, doi:10.1029/2001JD001443.

Clough, S. A., and M. J. Iacono (1995), Line-by-line calculation of atmospheric fluxes and cooling rates: 2. Application to carbon dioxide, ozone, methane, nitrous oxide and the halocarbons, *J. Geophys. Res.*, **100**(D8), 16,519–16,535.

Clough, S. A., M. W. Shephard, E. J. Mlawer, J. S. Delamere, M. J. Iacono, K. Cady-Pereira, S. Boukabara, and P. D. Brown (2004), Atmospheric radiative transfer modeling: A summary of the AER codes, *J. Quant. Spectrosc. Radiat. Transfer*, in press.

Dudhia, A., V. L. Jay, and C. D. Rodgers (2002), Microwindow selection for high-spectral-resolution sounders, *Appl. Opt.*, **41**(18), 3665–3673.

Echle, G., T. von Clarmann, A. Dudhia, J. M. Flaud, B. Funke, N. Glatthor, B. Kerridge, M. Lopez-Puertas, F. J. Martin-Torres, and G. P. Stiller (2000), Optimized spectral microwindows for data analysis of the Michelson Interferometer for Passive Atmospheric Sounding on the environmental satellite, *Appl. Opt.*, **39**(30), 5531–5540.

Jones, D. B. A., K. W. Bowman, P. I. Palmer, J. R. Worden, D. J. Jacob, R. N. Hoffman, I. Bey, and R. M. Yantosca (2003), Potential of observations from the Tropospheric Emission Spectrometer to constrain continental sources of carbon monoxide, *J. Geophys. Res.*, **108**(D24), 4789, doi:10.1029/2003JD003702.

Papoulis, A. (1984), *Probability, Random Variables and Stochastic Processes*, McGraw-Hill, New York.

Rodgers, C. D. (1998), Information content and optimization of high spectral resolution remote measurements, *Adv. Space Res.*, **21**(31), 361–367.

Rodgers, C. D. (2000), *Inverse Methods for Atmospheric Sounding: Theory and Practice*, World Sci., River Edge, N. J.

Rothman, L. S., et al. (1992), The Hitran Molecular Database—Editions of 1991 and 1992, *J. Quant. Spectrosc. Radiat. Transfer*, **48**(5–6), 469–507.

Tarantola, A. (1987), *Inverse Problem Theory: Methods for Data Fitting and Model Parameter Estimation*, Elsevier Sci., New York.

von Clarmann, T., and G. Echle (1998), Selection of optimized microwindows for atmospheric spectroscopy, *Appl. Opt.*, **37**(33), 7661–7669.

Worden, J. R., K. W. Bowman, and D. B. Jones (2004), Two dimensional characterization of atmospheric profile retrievals from limb sounding observations, *J. Quant. Spectrosc. Radiat. Transfer*, **86**(1), 45–71.

Yamaguchi, Y., A. B. Kahle, H. Tsu, T. Kawakami, and M. Pniel (1998), Overview of advanced spaceborne thermal emission and reflection radiometer (ASTER), *IEEE Trans. Geosci. Remote Sens.*, **36**(4), 1062–1071.

K. Bowman, S. S. Kulawik, H. Worden, and J. Worden, Jet Propulsion Laboratory, California Institute of Technology, 4800 Oak Grove Drive, Pasadena, CA 91109, USA. (john.worden@jpl.nasa.gov)

S. A. Clough and M. W. Shephard, Atmospheric and Environmental Research, Inc., 131 Hartwell Avenue, Lexington, MA 02421-3626, USA.
A. Goldman, Department of Physics, University of Denver, Denver, CO 80208, USA.